Enhanced Intertwined Spin and Charge Orders in the t–J Model in a Small J Case

Yu Zhang(张渝)[1], Jiawei Mei(梅佳伟)[1*], and Weiqiang Chen(陈伟强)[1,2*]

[1]*Department of Physics and Shenzhen Institute for Quantum Science and Engineering, Southern University of Science and Technology, Shenzhen 518055, China*
[2]*Shenzhen Key Laboratory of Advanced Quantum Functional Materials and Devices, Southern University of Science and Technology, Shenzhen 518055, China*

(Received 19 December 2022; accepted manuscript online 9 February 2023)

The one-band t–J model captures strong correlations in cuprate high-temperature superconductors. It accounts for the various intertwined spin and charge orders, and the superconductivity in the phase diagrams. To see the correlation effect on the intertwined orders, we implement the density matrix renormalization group method to simulate the t–J model in a small J case with $t/J = 10$, which is in a deeper Mott region than that with $t/J \simeq 3$ in cuprate superconducting compounds. We examine the results on a six-leg lattice with both the nearest and next-nearest-neighbor hoppings and antiferromagnetic coupling, and find the absence of superconductivity and enhanced intertwined spin and charge orders in the phase diagram. Besides the stripe phases, we find a new SDW + CDW phase in which the spin modulation is a (π, π) antiferromagnetism, while the wavelength of the charge modulation is shorter than that of the stripe phases. Our results suggest the enhanced intertwined orders and suppressed superconductivity in the deep Mott region.

DOI: 10.1088/0256-307X/40/3/037401

Since the discovery of cuprate high-temperature superconductor,[1] understanding its microscopic mechanism of superconductivity is a significant challenge in condensed matter physics.[2] Scientists have studied cuprate throughout the past few decades using a variety of cutting-edge experimental techniques and found various orders, including spin-density-wave (SDW), charge-density-wave (CDW), and stripe,[3] etc., besides the superconductivity.[2,4–10] These orders were referred as "intertwined orders",[4] since they may have an intimate connection with superconductivity, and studying them may help to understand the mechanism of cuprate high-temperature superconductivity. However, the general relationship between the intertwined orders and superconductivity is still debated. Since it is believed that the correlation effect plays a vital role in the mechanism of cuprate high-temperature superconductivity, a very natural question is how the intertwined orders and the superconductivity would be in the regime with a strong correlation effect, say the deeper Mott region.

While it is challenging to control correlations in the cuprate experimentally, we are ready to study the correlation effect in the numerical simulations. The one-band t–J model is believed to capture the main physics of the cuprate high-temperature superconductors.[11] Noticeably, various intertwined orders and superconductivity have been discovered in numerous numerical simulations, many of which have glaring similarities to the observed behaviors of cuprate.[12–23] For example, recent studies of the t–J model with $t/J = 3$ have observed superconductivity as well as some CDW and SDW orders, both on width-6 and width-8 cylinders in the region with $t_2/t_1 > 0$, which may relate to the electron doped cuprates.[22,23] Thus, it is a good platform to study the intertwined orders and superconductivity. The deeper Mott region corresponds to the small J case in the t–J model. Most of the studies on the t–J model focus on the regime with $t/J \simeq 3$, since the cuprate is also in this regime. Instead, in this Letter we would like to investigate the intertwined orders and superconductivity in the regime with $t/J = 10$. By comparing our results with the results in the literature at $t/J = 3$, we may answer the question of how the correlation effect affects the intertwined orders and superconductivity.

In this work, we use the density matrix renormalization group (DMRG) algorithm[24,25] to study a t–J model with both the nearest and next-nearest-neighbor hoppings (t_1 and t_2) and antiferromagnetic coupling (J_1 and J_2) with $t_1/J_1 = 10$ on a six-leg cylinder under periodic and open boundary conditions in the y and x directions, respectively. In comparison with the results at $t_1/J_1 = 3$ in the literature, we find that there is no superconducting (SC) phase at $t_1/J_1 = 10$, while there are three phases with different intertwined orders: two stripe phases and a phase with both SDW and CDW orders as shown in Fig. 1. Our results suggest that the intertwined orders are enhanced, while the superconductivity is suppressed by the correlation, which is consistent with some precious theoretical studies.[26,27] Specifically, we first give a brief overview of the t–J model. Then we show the ground state phase diagram of the model obtained from the DMRG calculations. The physical characteristics of each phase are next examined, including the charge density distribution, spin structure, and SC correlation.

Model and Method. We employ the DMRG to study the t–J model on a square lattice. The model reads

$$H = -\sum_{[ij]\sigma} t_{ij} P_{\mathrm{G}} \left(c^{\dagger}_{i\sigma} c_{j\sigma} + \mathrm{h.c.}\right) P_{\mathrm{G}} + \sum_{[ij]} J_{ij} \left(\boldsymbol{S}_i \cdot \boldsymbol{S}_j - \frac{n_i n_j}{4}\right), \tag{1}$$

where $c^{\dagger}_{i\sigma}$ and $c_{i\sigma}$ are the creation and annihilation operators for the electron with spin σ and at site i, respectively;

*Corresponding authors. Email: meijw@sustech.edu.cn; chenwq@sustech.edu.cn
© 2023 Chinese Physical Society and IOP Publishing Ltd

the Gutzwiller projector $P_{\rm G} = 1 - n_{i\uparrow}n_{i\downarrow}$ tracks the no-double-occupation condition; and $[ij]$ means a pair of site i and j. In the following, we consider only the nearest-neighbor (NN) coupling with $t_{\rm NN} = t_1$ and $J_{\rm NN} = J_1$, and the next-nearest-neighbor (NNN) coupling with $t_{\rm NNN} = t_2$ and $J_{\rm NNN} = J_2$. We focus on the case with $J_1 = 0.1t_1$, $0 \leq t_2/t_1 \leq 0.3$, $J_2/J_1 = (t_2/t_1)^2$, and the hole doping $1/12 \leq \delta \leq 1/3$.

In the calculation, we consider a six-leg ladder with a length up to $L_x = 48$ under a periodic boundary in the y direction and an open boundary in the x direction. We use a finite system DMRG algorithm with $U(1)$ symmetry to study the system by using the ITensor library.[28] As a benchmark, we calculate the case with $t/J = 3$, and the results are consistent with the ones in Ref. [22]. Then, we focus on the case with $t_1/J_1 = 10$ in the deep Mott region. We perform 60 sweeps and keep up to $D = 8000$ states in most of the results. For some important points such as $\delta = 1/12$, $t_2/t_1 = 0.3$, and $\delta = 1/8$, $t_2/t_1 = 0.3$, we keep the bond dimensions up to $D = 14000$.

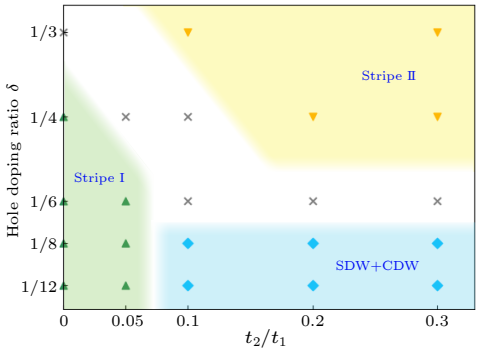

Fig. 1. The phase diagram in t_2–δ plane with t_2 representing the next-nearest-neighbor hopping and δ the doping concentration. The green, yellow, and blue regions indicate stripe I phase, stripe Ⅱ phase, and SDW + CDW phase, respectively.

Results and Discussions. The main result of this study is the phase diagram shown in Fig. 1. We identify three different phases, i.e., the stripe I phase, stripe Ⅱ phase, and the SDW + CDW phase, in the case of $t_1/J_1 = 10$. Unfortunately, we do not find the SC phase in our phase diagram. The SDW + CDW phase has the SDW order with the wave vector pinning at the antiferromagnetic vector $\boldsymbol{Q}_{\rm AF} = (\pi, \pi)$ and the CDW order with the charge modulation length $\lambda_{\rm cdw} \simeq \frac{2}{L_y\delta}$. The two stripe phases have the intertwined SDW order with an incommensurate wave vector away from $\boldsymbol{Q}_{\rm AF}$ and the CDW order with the SDW and CDW modulation wavelength $\lambda_{\rm sdw} = 2\lambda_{\rm cdw}$. The stripe I phase has $\lambda_{\rm cdw} \simeq \frac{4}{L_y\delta}$, which has also been observed in the $t_1/J_1 = 3$ case in small doping and small t_2/t_1 ratio.[22] The stripe Ⅱ phase has $\lambda_{\rm cdw} \simeq \frac{6}{L_y\delta}$. The SC correlation decays exponentially with distance in all the three phases, though it decays more slowly in the SDW + CDW phase than that in the stripe phases.

Our results suggest that in the deeper Mott region ($t/J = 10$), different from in the $t/J = 3$ case, the intertwined orders dominate in the parameter regime we studied, while the superconductivity is strongly suppressed by the strong correlation. In the following, we present the details of the characterizations of these phases.

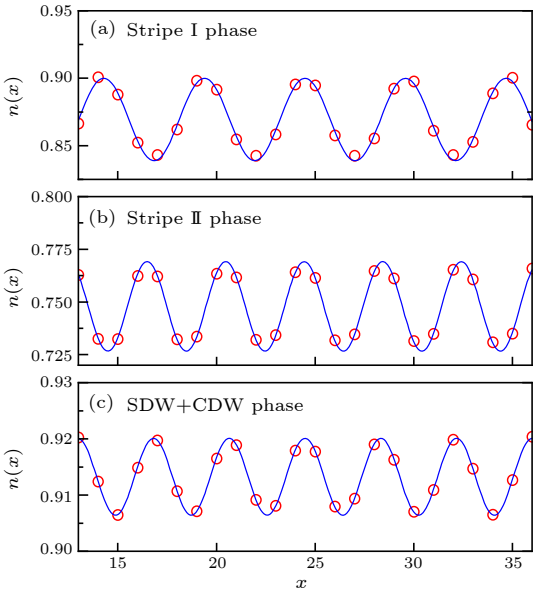

Fig. 2. Charge density distribution. The charge density distributions $n(x) = \frac{1}{L_y}\sum_{y=1}^{L_y} n(x, y)$ for (a) $t_2/t_1 = 0.0$, $\delta = 1/8$ (stripe I phase), (b) $t_2/t_1 = 0.3$, $\delta = 1/4$ (stripe Ⅱ phase), (c) $t_2/t_1 = 0.3$, $\delta = 1/12$ (SDW + CDW phase). The blue lines are fitting curves to the function $n(x) = n_0 + A_{\rm cdw}\cos(Q_{\rm cdw}x + \phi_{\rm cdw})$.

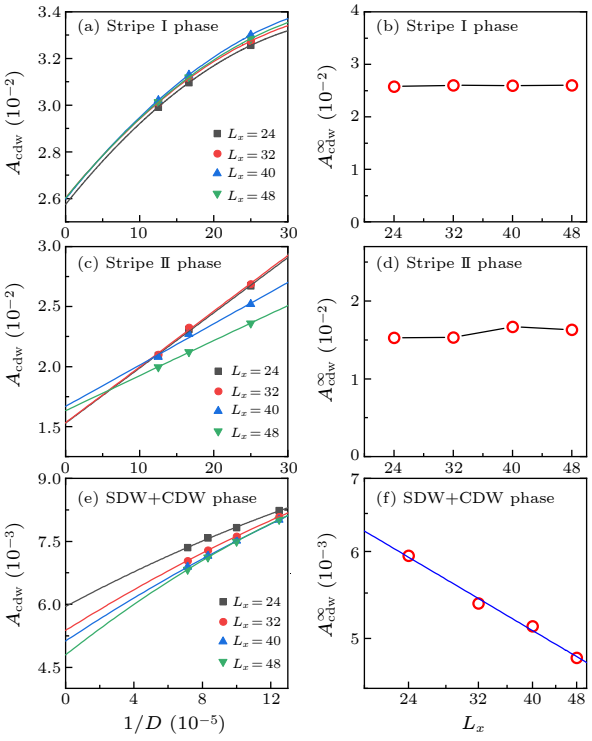

Fig. 3. CDW amplitude. The amplitude $A_{\rm cdw}$ for (a) $t_2/t_1 = 0.0$, $\delta = 1/8$ (stripe I phase), (c) $t_2/t_1 = 0.3$, $\delta = 1/4$ (stripe Ⅱ phase), (e) $t_2/t_1 = 0.3$, $\delta = 1/12$ (SDW + CDW phase) with different dimensions. D is the $U(1)$ bond dimension, which corresponds to $D = 4000$, 6000, 8000 here (for SDW + CDW phase, $D = 8000$, 10000, 12000, 14000). Finite-size scaling $A_{\rm cdw}(L_x)$ for (b) $t_2/t_1 = 0.0$, $\delta = 1/8$ (stripe I phase), (d) $t_2/t_1 = 0.3$, $\delta = 1/4$ (stripe Ⅱ phase), (f) $t_2/t_1 = 0.3$, $\delta = 1/12$ (SDW + CDW phase). Please note that a double-logarithmic plot is provided in (f).

Figure 2 displays the charge density modulation

$$n(x) = \frac{1}{L_y}\sum_{y=1}^{L_y} n(x,y), \tag{2}$$

along the x direction in different phases. In order to avoid the boundary effects, we only use the data of the lattice sites with $\frac{L_x}{4}+1 \le i_x \le \frac{3L_x}{4}$ for fitting. The typical results of $n(x)$ vs x can be well fitted by the function $n(x) = n_0 + A_{\rm cdw}\cos(Q_{\rm cdw}x + \phi_{\rm cdw})$, from which we identify the charge modulation wavelength ($\lambda_{\rm cdw} = \frac{2\pi}{Q_{\rm cdw}}$) and the amplitude $A_{\rm cdw}$. For different doping concentrations δ, different phases have different charge modulation wavelengths, $\lambda_{\rm cdw} \simeq \frac{4}{L_y\delta}$ in the stripe I phase [Fig. 2(a)], $\lambda_{\rm cdw} \simeq \frac{6}{L_y\delta}$ in the stripe Ⅱ phase [Fig. 2(b)], and a shorter wavelength $\lambda_{\rm cdw} \simeq \frac{2}{L_y\delta}$ in the SDW + CDW phase [Fig. 2(c)].

Figure 3 shows the dependences of the charge modulation amplitude $A_{\rm cdw}$ on bond dimension D and size length L_x. In the left column of Fig. 3, we fit the CDW amplitude $A_{\rm cdw}$ by the polynomial function $A_{\rm cdw} = A^{\infty}_{\rm cdw} + a/D + b/D^2$. The dependence of the $A^{\infty}_{\rm cdw}$ vs the length of the ladder L_x is shown in the right column of Fig. 3. The charge modulation of the two stripe phases is almost size-independent, which suggests a stable CDW order. For the SDW + CDW phase, the $A^{\infty}_{\rm cdw}$ decays in power-law form $A_{\rm cdw}(L_x) \propto L_x^{-K_c/2}$ with $K_c \simeq 0.6$, which suggests that there is a quasi-long-rang CDW order in this phase.

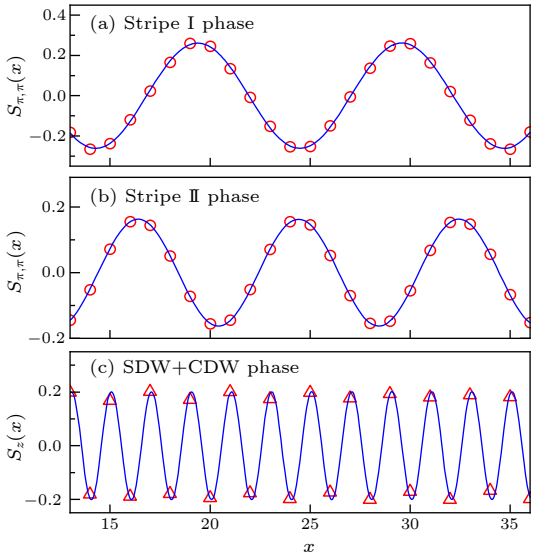

Fig. 4. Spin structure. The $S_{\pi,\pi}(x)$ distribution for (a) $t_2/t_1 = 0.0$, $\delta = 1/8$ (stripe I phase), (b) $t_2/t_1 = 0.3$, $\delta = 1/4$ (stripe Ⅱ phase). (c) The spin $S_z(x)$ distribution of a chain ($y = 1$) for $t_2/t_1 = 0.3$, $\delta = 1/8$ (SDW + CDW phase).

Next, we show the results of the spin modulations of the three phases. One straightforward way is to measure the spin $S_z = (n_{i\uparrow} - n_{i\downarrow})/2$, as shown in Fig. 4(c) for the SDW + CDW phase. For the two stripe phases in Figs. 4(a) and 4(b), we can define [19]

$$S_{\pi,\pi}(x) = 1/L_y\sum_{y=1}^{L_y}(-1)^{x+y}S_z(x,y), \tag{3}$$

to eliminate the embedding antiferromagnetic background. While the spin modulation for the SDW + CDW phase is pinned at the antiferromagnetic wave vector $\boldsymbol{Q}_{\rm AF} = (\pi,\pi)$ as $S_z = A_{\rm sdw}\cos(\pi x + \pi y)$ in Fig. 4(c) (where the y-dependence is not shown), the two stripe phases have an incommensurate spin wave vector $Q_{\rm sdw}$ away from $\boldsymbol{Q}_{\rm AF}$, and $S_{\pi,\pi}(x)$ can be fitted by the function $S_{\pi,\pi}(x) = A_{\rm sdw}\cos(Q_{\rm sdw}x + \phi_{\rm sdw})$ as shown in Figs. 4(a) and 4(b), giving rise to a spin modulation wavelength $\lambda_{\rm sdw} \simeq \frac{8}{L_y\delta}$ and $\lambda_{\rm sdw} \simeq \frac{12}{L_y\delta}$ in the stripe I and stripe Ⅱ phases, respectively. Here $\lambda_{\rm sdw} = 2\lambda_{\rm cdw}$ in the stripe phases. The corresponding SDW amplitude $A_{\rm sdw}$ depending on bond dimension D and size length L_x is shown in Fig. 5. The spin modulations of the two stripe phases are almost size-independent, suggesting a stable SDW order. The $A^{\infty}_{\rm sdw}$ in the SDW + CDW phase increases with L_x, implying a more stable SDW order.

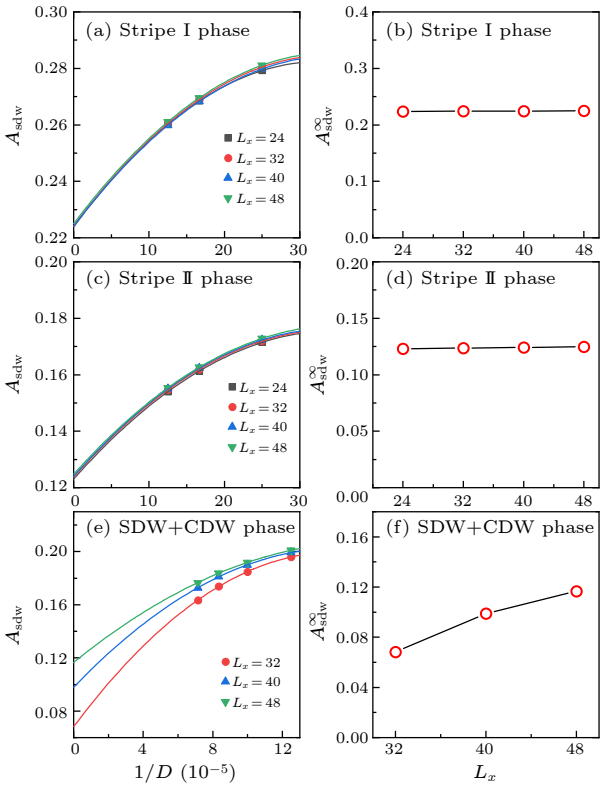

Fig. 5. SDW amplitude. The amplitude $A_{\rm sdw}$ for (a) $t_2/t_1 = 0.0$, $\delta = 1/8$ (stripe I phase), (c) $t_2/t_1 = 0.3$, $\delta = 1/4$ (stripe Ⅱ phase), (e) $t_2/t_1 = 0.3$, $\delta = 1/12$ (SDW + CDW phase). D is the $U(1)$ bond dimension, which corresponds to $D = 4000, 6000, 8000$ in (a) and (c), and $D = 8000, 10000, 12000, 14000$ in (e). Finite-size scaling $A_{\rm sdw}(L_x)$ for (b) $t_2/t_1 = 0.0$, $\delta = 1/8$ (stripe I phase), (d) $t_2/t_1 = 0.3$, $\delta = 1/4$ (stripe Ⅱ phase), (f) $t_2/t_1 = 0.3$, $\delta = 1/12$ (SDW + CDW phase).

Finally, we examine the SC correlation of the three phases by studying the pairing correlation

$$P_{\alpha\beta}(x,y_0) = \langle \Delta^{\dagger}_{\alpha}(x_0,y_0)\Delta_{\beta}(x_0+x,y_0)\rangle, \tag{4}$$

where the bond orientations are designated $\alpha = x/y$, and $\Delta^{\dagger}_{\alpha}(x,y)$ is the spin-singlet pair-field creation operator given by

$$\Delta^{\dagger}_{\alpha}(x,y) = \frac{1}{\sqrt{2}}\left[c^{\dagger}_{(x,y)\uparrow}c^{\dagger}_{(x,y)+\alpha\downarrow} - c^{\dagger}_{(x,y)\downarrow}c^{\dagger}_{(x,y)+\alpha\uparrow}\right]. \tag{5}$$

Figure 6 is the position x-dependence of the extrapolated P_{yy} in the $D = \infty$ limit which collapses to the exponential decay function $P_{yy} \propto \exp(-x/\xi_{sc})$ in the long distance with the SC correlation length $\xi_{sc} \simeq 0.9$, $\xi_{sc} \simeq 1.8$, and $\xi_{sc} \simeq 3.5$ for the stripe I phase, the stripe Ⅱ phase, and the SDW + CDW phase, respectively. The exponential decay of the SC correlation over distance indicates the absence of long-range SC order in all the three phases.

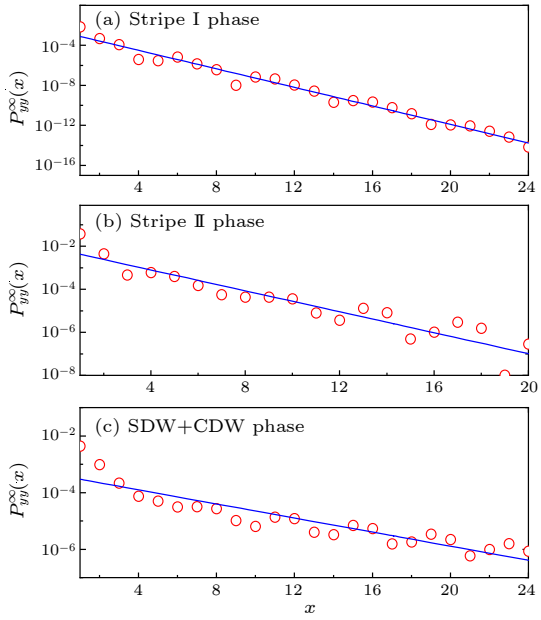

Fig. 6. SC correlation. Semi-logarithmic plot of SC correlation P_{yy} for $D = \infty$ for (a) $t_2/t_1 = 0.0$, $\delta = 1/8$ (stripe I phase), (b) $t_2/t_1 = 0.3$, $\delta = 1/4$ (stripe Ⅱ phase), (c) $t_2/t_1 = 0.3$, $\delta = 1/12$ (SDW + CDW phase). The blue line is fitting curves for exponentially decay $P_{yy} \propto \exp(-x/\xi_{sc})$.

In conclusion, we have investigated the ground states of the deep Mott region ($t_1/J_1 = 10$) with the six-leg cylinder t–J model using DMRG calculations. It is found that there are three phases with intertwined orders: two stripe phases and one phase with both SDW and CDW orders. The superconductivity is not present in all the three phases, either. In the stripe I phase, there is a charge modulation with wavelength $\lambda \simeq \frac{4}{L_y\delta}$ and a spin modulated with wavelength $\lambda \simeq \frac{8}{L_y\delta}$. As we can see, the wavelength of the spin order is twice the charge order.[29] The stripe Ⅱ phase is similar to the stripe I phase, but has different wavelengths of charge modulation and spin modulation of $\lambda \simeq \frac{6}{L_y\delta}$ and $\lambda \simeq \frac{12}{L_y\delta}$, respectively. In the SDW + CDW phase, we find a charge modulation with wavelength $\lambda \simeq \frac{2}{L_y\delta}$, while the spin modulation is a (π, π) antiferromagnetism. Our results suggest that the intertwined orders are enhanced and superconductivity is suppressed in the deep Mott region.

Acknowledgement. We acknowledge discussions with Shoushu Gong. This work was supported by the National Key R&D Program of China (Grant No. 2022YFA1403700), the National Natural Science Foundation of China (Grant No. 12141402), the Science, Technology and Innovation Commission of Shenzhen Municipality (Grant No. ZDSYS20190902092905285), Guangdong Basic and Applied Basic Research Foundation (Grant No. 2020B1515120100), and Center for Computational Science and Engineering at Southern University of Science and Technology.

References

[1] Bednorz J G and Müller K A 1986 *Z. Phys. B: Condens. Matter* **64** 189
[2] Keimer B, Kivelson S A, Norman M R, Uchida S, and Zaanen J 2015 *Nature* **518** 179
[3] Emery V, Kivelson S, and Tranquada J 1999 *Proc. Natl. Acad. Sci.* **96** 8814
[4] Fradkin E, Kivelson S A, and Tranquada J M 2015 *Rev. Mod. Phys.* **87** 457
[5] Armitage N, Fournier P, and Greene R 2010 *Rev. Mod. Phys.* **82** 2421
[6] Damascelli A, Hussain Z, and Shen Z X 2003 *Rev. Mod. Phys.* **75** 473
[7] Norman M and Pépin C 2003 *Rep. Prog. Phys.* **66** 1547
[8] Shen K M and Davis J S 2008 *Mater. Today* **11** 14
[9] Chu C W, Deng L Z, and Lv B 2015 *Physica C* **514** 290
[10] Comin R and Damascelli A 2016 *Annu. Rev. Condens. Matter Phys.* **7** 369
[11] Zhang F C and Rice T M 1988 *Phys. Rev. B* **37** 3759
[12] Corboz P, Rice T M, and Troyer M 2014 *Phys. Rev. Lett.* **113** 046402
[13] Dodaro J F, Jiang H C, and Kivelson S A 2017 *Phys. Rev. B* **95** 155116
[14] Jiang H C, Weng Z Y, and Kivelson S A 2018 *Phys. Rev. B* **98** 140505
[15] Corboz P, White S R, Vidal G, and Troyer M 2011 *Phys. Rev. B* **84** 041108
[16] Izyumov Y A 1997 *Phys.-Usp.* **40** 445
[17] White S R and Scalapino D 2009 *Phys. Rev. B* **79** 220504
[18] Himeda A, Kato T, and Ogata M 2002 *Phys. Rev. Lett.* **88** 117001
[19] White S R and Scalapino D J 1998 *Phys. Rev. Lett.* **80** 1272
[20] White S R and Scalapino D 1999 *Phys. Rev. B* **60** R753
[21] Sorella S, Martins G, Becca F, Gazza C, Capriotti L, Parola A, and Dagotto E 2002 *Phys. Rev. Lett.* **88** 117002
[22] Gong S S, Zhu W, and Sheng D N 2021 *Phys. Rev. Lett.* **127** 097003
[23] Jiang S T, Scalapino D J, and White S R 2021 *Proc. Natl. Acad. Sci. USA* **118** e2109978118
[24] White S R 1992 *Phys. Rev. Lett.* **69** 2863
[25] White S R 1993 *Phys. Rev. B* **48** 10345
[26] Poilblanc D and Rice T 1989 *Phys. Rev. B* **39** 9749
[27] Zaanen J and Gunnarsson O 1989 *Phys. Rev. B* **40** 7391
[28] Fishman M, White S R, and Stoudenmire E M 2020 arXiv:2007.14822 [cs.MS]
[29] Kivelson S A, Bindloss I P, Fradkin E, Oganesyan V, Tranquada J M, Kapitulnik A, and Howald C 2003 *Rev. Mod. Phys.* **75** 1201